A TIME-DISCRETE MODEL FOR DYNAMIC FRACTURE BASED ON CRACK REGULARIZATION

BLAISE BOURDIN, CHRISTOPHER J. LARSEN, AND CASEY L. RICHARDSON

Abstract. We propose a discrete time model for dynamic fracture based on crack regularization. The advantages of our approach are threefold: first, our regularization of the crack set has been rigorously shown to converge to the correct sharp-interface energy [2, 3]; second, our condition for crack growth, based on Griffith's criterion, matches that in quasi-static settings [7], where Griffith originally stated his criterion; third, solutions to our model converge, as the time-step tends to zero, to solutions of the correct continuous time model [25]. Furthermore, in implementing this model, we naturally recover several features, such as the elastic wave speed as an upper bound on crack speed, and crack branching for sufficiently rapid boundary displacements. We conclude by comparing our approach to so-called "phase-field" ones. In particular, we explain why phase-field approaches are good for approximating free boundaries, but not the free discontinuity sets that model fracture.

1. Introduction

Griffith's criterion for quasi-static of brittle materials [20] supposes that as a crack grows, the displacement field is instantly in a new equilibrium, with a resulting decrease in stored elastic energy that matches the surface energy of the crack increment. More precisely, a crack propagates if the rate of elastic energy decrease per unit area of increment, equals the (quasi-static) *critical energy release rate*. It stalls if the elastic energy release rate is less than that critical rate. It is unstable if the release rate exceeds the critical rate [27, Secs. 1.2 and 4]. For isotropic linear materials, this critical energy release rate is linked to the *stress intensity factors* by Irwin's formula, and we refer to it as the *fracture toughness* in this context.

Making this principle mathematically precise began with Ambrosio & Braides [1] in the static case and gradient flows, extended to quasi-static evolutions by Francfort & Marigo [17]. They proposed minimizing the sum of stored elastic energy and surface energy of discontinuity sets, to obtain displacements that are stable in the sense of Griffith. That is, for displacements $u \in SBV(\Omega)$, the space of *special functions of bounded variation*, with Ω representing the reference configuration of a body (u taking real values, modeling antiplane displacement), they consider energy functionals of the form

$$E(u) := \frac{1}{2}\mu \int_\Omega |\nabla u|^2 dx + G_c \mathcal{H}^{N-1}(S(u)).$$

Here μ is the shear modulus of the considered material, G_c is its fracture toughness, $S(u)$ denotes the discontinuity set of u, $\mathcal{H}^{N-1}$ is the $N-1$ dimensional Hausdorff measure, and the minimization is subject to a Dirichlet condition on a part $\partial\Omega_D$ of its boundary while the remaining part $\partial\Omega_N := \partial\Omega \setminus \partial\Omega_D$ remains traction-free. The idea is that, if u is a minimizer of E, then it is stable in the sense of Griffith as adding any increment to its crack set $S(u)$ cannot reduce the stored elastic energy by more than the cost of the increment.

We introduce a discrete time model for brittle fracture dynamics, based on only two principles: First, the displacement u should follow elastodynamics off the crack, and second, the crack should grow based only on the stress at the crack "tip" together with the material properties at the tip, in a way that is consistent with Griffith's criterion for crack growth. Our guiding principle for crack growth is, if the elastic field near the crack is such that the crack would grow based on Griffith's quasi-static criterion, then the crack should also grow, in the same infinitesimal way, if the stresses are due to elastodynamics.

Putting this criterion on a precise mathematical footing is considerably more difficult than the quasi-static formulation of [17]. The reason is that Griffith's criterion in the quasi-static setting is

in essence an energy comparison – for a potential crack increment ΔC, there is a corresponding and *instantaneous* decrease in stored elastic energy. The length, or surface energy, of the crack increment can be compared with the elastic decrease, and the increment that results in the best, and sufficiently large, elastic reduction is deemed to be the actual crack increment.

Extending this principle to dynamics is not straightforward, since crack increments do not result in instantaneous decreases in stored elastic energy (and the effect on kinetic energy is expected to be an increase). There is, however, a rigorous approximation procedure for quasi-static fracture based on a regularization of the crack [2, 3], where the energy functional

$$E_\varepsilon(u,v) := \int_\Omega \left(v^2+\eta_\varepsilon\right)|\nabla u|^2\,dx + \int_\Omega \frac{(1-v)^2}{4\varepsilon} + \varepsilon\,|\nabla v|^2\,dx, \tag{1}$$

is shown to be an approximation of the total elastic energy plus the surface energy of a crack K:

$$E(u,K) := \int_{\Omega\setminus K} |\nabla u|^2\,dx + \mathcal{H}^{N-1}(K).$$

Formally, when ε is "small", the second term in (1) forces v to be close to one except on a small set, an approximation of K, while the first term allows u to have large variation where v is close to zero.

In our approach, the energy corresponding to the phase-field function, v, is minimized at each discrete time (subject to irreversibility constraints as in [7, 18]), while the displacement u follows dynamics, affected by v only on a small set modeling the crack, where u is allowed to be discontinuous. More precisely, given $u(x,0) = u_0(x)$, $u_t(x,0) = u_1(x)$, we first solve for $v(x,0)$ by minimizing $v \mapsto E_\varepsilon(u_0,v)$. The dynamics are governed by

$$u_{tt} - \operatorname{div}\left[\left(v^2+\eta_\varepsilon\right)\nabla u\right] = f, \tag{2}$$

where f is the applied load. To find $u(x,\Delta t)$, we do one time step in (2) starting at time zero and using $v = v(x,0)$. This gives $u(x,\Delta t)$, and $v(x,\Delta t)$ is then found by minimizing $v \mapsto E_\varepsilon(u(x,\Delta t),v)$, etc. The corresponding continuous-time model is

$$u_{tt} - \operatorname{div}\left[\left(v^2+\eta_\varepsilon\right)\nabla u\right] = f,$$

together with

$$v \in \operatorname{argmin} E_\varepsilon(u,\cdot),\ v \text{ decreasing in time.}$$

In fact, we also get (see [25]) that the total energy (including the energy dissipated in forming the crack) is constant in time, and that solutions to our discrete-time model converge to solutions of this continuous-time model as the time step goes to zero. For a discussion of corresponding sharp-interface models, see [26].

2. The Discrete Time Model

Let $\Omega \subset \mathbb{R}^N$ be a bounded connected domain with Lipschitz boundary. As in [16], we enforce boundary conditions by considering an extended domain Ω', bounded and open with Lipschitz boundary, such that $\overline{\Omega} \subset \Omega'$.

In this section, we will describe our algorithm for computing the evolution of cracks in the case of dynamic antiplane shear. As described in the introduction the idea of this computational model is to describe the evolution of the system "away from the crack" by a PDE governing the dynamics of an elastic body, and combine this with an evolution law for the crack set based on minimizing an energy motivated by Griffith.

Specifically, given boundary conditions $g \in H^1(\Omega')$, a static model of antiplane shear with fracture is given by minimizing

$$E(u) := \frac{\mu}{2}\int_\Omega |\nabla u|^2\,dx + G_c\mathcal{H}^{N-1}(S(u))$$

over $u \in SBV(\Omega)$ with $u = g$ in $\Omega' \setminus \Omega$, μ and G_c being the shear modulus and fracture toughness of the homogeneous, isotropic material considered. Following [7] and [8], we define an Ambrosio-Tortorelli approximation of this static energy. We introduce

$$F(u,v) := \begin{cases} E(u) & \text{if } v \equiv 1, \\ +\infty & \text{otherwise.} \end{cases}$$

Then, for any $\varepsilon > 0$ and $\eta_\varepsilon << \varepsilon$, define the functionals

$$E_\varepsilon(u,v) := \frac{\mu}{2}\int_\Omega \left(v^2+\eta_\varepsilon\right)|\nabla u|^2\,dx + G_c\int_{\Omega'\setminus\partial\Omega_N}\frac{(1-v)^2}{4\varepsilon}+\varepsilon\,|\nabla v|^2\,dx.$$

and

$$F_\varepsilon(u,v) := \begin{cases} E_\varepsilon(u,v) & \text{if } u\in W^{1,2}(\Omega'\setminus\partial\Omega_N;\mathbb{R});\ v\in W^{1,2}(\Omega'\setminus\partial\Omega_N),\\ +\infty & \text{otherwise.}\end{cases}$$

It is a well known result that

$$F_\varepsilon \xrightarrow{\Gamma} F \quad \text{as } \varepsilon\to 0,$$

which implies, using a classical argument for Γ–convergence [11, 14], that the minimizers of F_ε converge to that of F as $\varepsilon\to 0$.

In the dynamic case, we have a time dependent loading given by $g\in L^\infty\left([0,T];L^\infty(\Omega')\right)\cap W^{1,1}\left([0,T];W^{1,1}(\overline{\Omega})\right)$. As in [7], we note that for fixed u, $F_\varepsilon(u,\cdot)$ is strictly convex and that the unique minimizing v can be directly computed. Thus, for any $\varepsilon>0$, and given an intial condition $u_\varepsilon(x;0)$ such that $u_\varepsilon(x;0)=g(x;0)$ in $\Omega'\setminus\Omega$, we find $v_\varepsilon(x;0)$ by

$$v_\varepsilon(x;0) = \operatorname*{argmin}_v F_\varepsilon(u_\varepsilon(x;0),v).$$

Then, we advance the elastic dynamics by a finite difference discretization of the PDE

$$\rho(u_\varepsilon)_{tt} = \mu\,\mathrm{div}\left[\left(v_\varepsilon^2+\eta_\varepsilon\right)\nabla u_\varepsilon\right], \tag{3}$$

where ρ is the density of the material we consider.

In order to obtain a stable scheme, we use backward differences in time: we consider the time range $(0,T)$ discretized into N intervals of length $\delta_t = T/N$, and set

$$(u_\varepsilon)_t(x;t) = \frac{u_\varepsilon(x;t)-u_\varepsilon(x,t-\delta_t)}{\delta_t},$$

and

$$(u_\varepsilon)_{tt}(x;t) = \frac{u_\varepsilon(x;t)-2u_\varepsilon(x,t-\delta_t)+u_\varepsilon(x,t-2\delta_t)}{\delta_t^2}.$$

After some simple algebra, the discrete version of (3) becomes then

$$\rho(u_\varepsilon)(x;t) - \mu\delta_t^2\,\mathrm{div}\left[\left(v_\varepsilon^2+\eta_\varepsilon\right)\nabla u_\varepsilon(x;t)\right] = 2u_\varepsilon(x;t-\delta_t)-u_\varepsilon(x,t-2\delta_t). \tag{4}$$

We repeat this process for each timestep. The steps of this computational model are summarized in Algorithm 1.

Algorithm 1 Time–discrete algorithm

Require: $u_\varepsilon(x;0)$, $(u_\varepsilon)_t(x;0)$, $\delta_t = T/N$
1: Set $u_\varepsilon(x;-\delta_t) = \delta_t(u_\varepsilon(x;0)-(u_\varepsilon)_t(x;0))$.
2: **for** $i=1$ to N **do**
3: Set $t=i\delta_t$.
4: Find u_ε solution of (4).
5: Find $v_\varepsilon(x,t)\in H^1(\Omega')$ minimizing $F_\varepsilon(u_\varepsilon(x;t),v)$ under the irreversibility constraint $v(x)=0$ on $\{x\,;\,v_\varepsilon(x;t-\delta_t)\le\alpha_\varepsilon\}$
6: **end for**

Note that at each time step, one now needs to solve two linear elliptic problems instead of only one for the v–minimization. The additional cost of such an implicit scheme is offset by an increased stability and scalability when implemented in parallel supercomputers (see for instance [24]).

A critical choice in the numerical implementation of the discrete model is the hyperbolic solver for the u–step (4). Our numerical implementation is derived from the quasi-static model, as presented in [8, 7, 9]. It is based on linear finite elements, and the underlying infrastructure for the parallel implementation on supercomputers is provided by PETSc [6, 5]. Linear finite elements may not be the most appropriate discretization scheme for the u–step. However, as the scope of this study is to give a quick insight on the properties of our model, we do not believe that this is a problem at this

stage. Of course, a more suited numerical method (using a discontinuous Galerkin or a finite volume based discretization, for instance) will be studied in the future. For the same reason, we restricted ousrselves to the antiplane shear case. Implementing the model in the two and three dimensional elasticity case does not raise any additional difficulty, but increases the cost of the investigative numerical work we performed.

3. Experiments

3.1. **Some properties of the hyperbolic solver.** Before conducting dynamic fracture experiments, we seek to illustrate the adequacy of our numerical approach. For that matter, we conducted a series of simple computations, on an essentially unidimensional problem. Consider a rectangular domain $\Omega = (0,1) \times (0,.05)$. To its left edge, we apply a time-dependent Dirichlet boundary condition $g(y;t)$ given by

$$g(y;t) = \begin{cases} \frac{1}{2}\left(1 - \cos(\pi t/t_l)\right) & \text{if } t \le t_l \\ g_0 & \text{if } t > t_l, \end{cases}$$

with $g_0 = 1$ and $t_l = .1$. We prescribed a null displacement boundary condition on the right edge, while the upper and lower edge are left free. The material properties are $\mu = 1$ (corresponding to an idealized homogeneous isotropic material with $E = 2$ and $\nu = 0$), $\rho = 1$. We set the fracture toughness G_c to 10, high enough that the domain remains purely elastic. For such a loading, the elasto-dynamic displacement consists in a single smooth transverse wave traveling at speed $\omega = \sqrt{\mu/\rho} = 1$, and reflecting on the left and right edges. Figure 1 represents the evolution of the bulk, surface and kinetic energies as a function of time for various values of the time step δ_t. All computations were performed on a Delaunay-Voronoi mesh of size $h = 2.5E-2$, consisting of approximately 25,000 vertices and 50,000 elements. As we expected, the numerical scheme is dissipative (see how the total energy decays after the initial loading phase), and the amount of dissipation decreases with the time step. As δ_t becomes small compared to h, the computed solution develops high frequency oscillations, leading to the small amplitude, high frequency oscillations of the individual components of the energy for $\delta_t = 1\mathrm{E}-4$. This is also expected, as the smoothing effect of the second order term in (4) vanishes when $\delta_t \to 0$.

We then studied the dispersivity of our numerical scheme. Figure 2 compares the profile of the deformation field as the traveling wave crosses the midline of the domain, traveling to the right, for the first, second and third time. The parameters correspond to that of Figure 1 (bottom-left). That the profile spreads out is consistent with the presence of the smoothing term on the left hand side of (4), and the loss of bulk energy highlighted in Figure 1 as time increases. Notice however how the peaks of the bulk and kinetic energies in Figure 1 are 1 unit of time apart, which is consistent with a transverse wave speed of 1 and a domain length of 1.

3.2. **A tearing experiment.** One of the strengths of the variational approach is its ability to consider *any* crack path, including kinking, branching, nucleation etc. In some cases (typically a subset of crack evolution labelled as *unstable* in the classical Griffith-type analysis), this can lead to unphysical evolutions. An example of such an evolution is the antiplane tearing experiment presented in detail in [9], and which we revisit here.

Consider a rectangular domain occupying the domain $(0,L) \times (-H,H)$, and assume $H \ll L$. To its left edge, one applies a monotonically increasing mode-III displacement $g(x,y;t) = g_0(t)\,\mathrm{sgn}(y)$ along the z–axis, sgn representing the sign function, and $g_0(t)$ an arbitrary monotonically increasing function. Additionally, we consider only single cracks occupying the region $(0,l(t)) \times \{0\}$ along the domain's symmetry axis. Figure 3(left), adapted from [9], represents the evolution of the bulk, surface and total energies as a function of t for this problem. As the magnitude of the fixed displacement increases, the crack grows linearly until it reaches a critical length $l_V \sim L/2$ then propagates *instantly* throughout the remaining half of the domain. The paradox here is not as much the instant propagation as it is the value of the threshold l_V. Indeed, the crack tip has to "know" when it has reached the mid-point. This is especially puzzling in the one dimensional limit (*i.e.* as $H/L \to 0$), as the displacement field for $0 \le x \le l(t)$ does not depend on L but $l_V = L$. Note that going

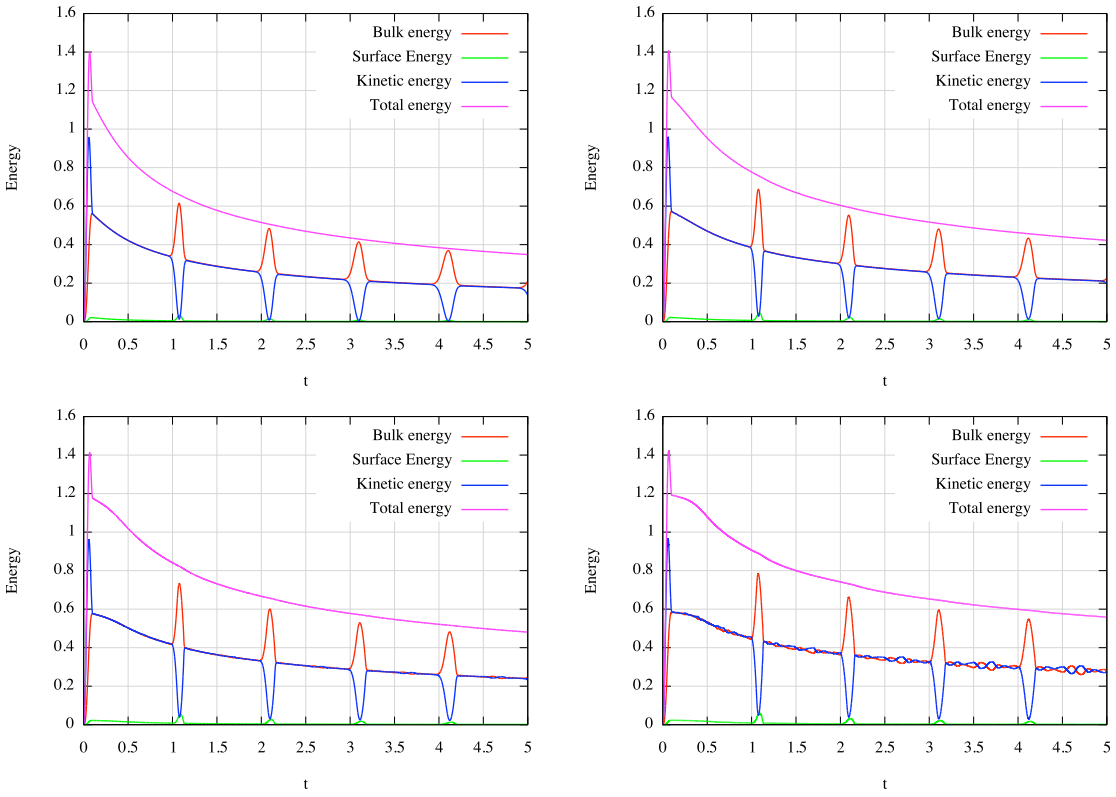

FIGURE 1. Evolution of the bulk, surface, kinetic and total energies for $\delta_t = 1\mathrm{E}-3$ (top left), $\delta_t = 5\mathrm{E}-4$ (top right), $\delta_t = 2.5\mathrm{E}-4$ (bottom left) and $\delta_t = 1\mathrm{E}-4$ (bottom right).

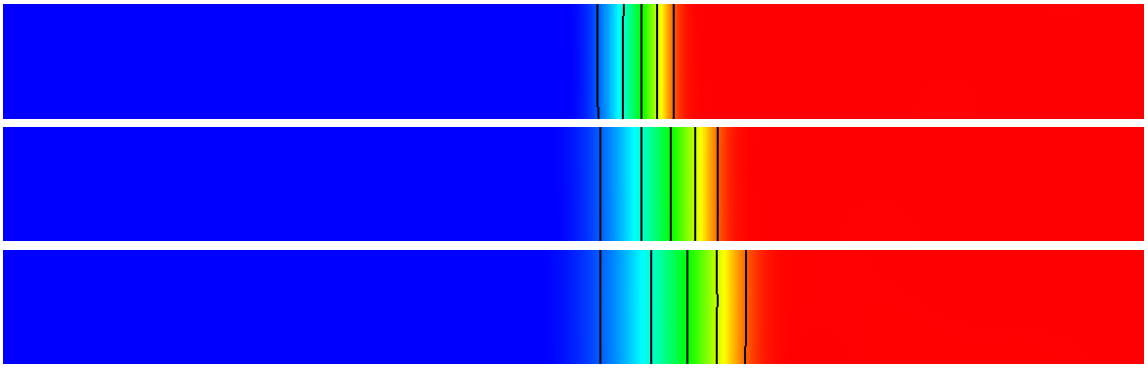

FIGURE 2. Profile of the deformation field at $t =$ and $t =$, as the elastic wave crosses the midline of the domain traveling left to right. The color field corresponds to the value of u. In order to facilitate the comparison of the profile, a few level lines have been added.

back to the classical Griffith theory does not address this issue in a satisfying way. In the classical framework, the crack tip also propagates at a constant speed until it reaches a threshold $l_G > l_V$, corresponding to a displacement magnitude t_V. For $t > t_V$, Griffith's criterion *cannot be satisfied*. From the variational standpoint, the only local minimizers of E_ε for $t > t_G$ corresponds again to a crack propagating instantly throughout the domain. The paradox here is that this cannot be accomplished while preserving the total energy (see Figure 3(right)). That the Ambrosio-Tortorelli–based approach approximates this crack evolution is also somewhat unexpected since there is no guarantee

a priori that the local minimizers of the regularized energy converge to that of the variational one (for $l_V \leq l \leq l_G$).

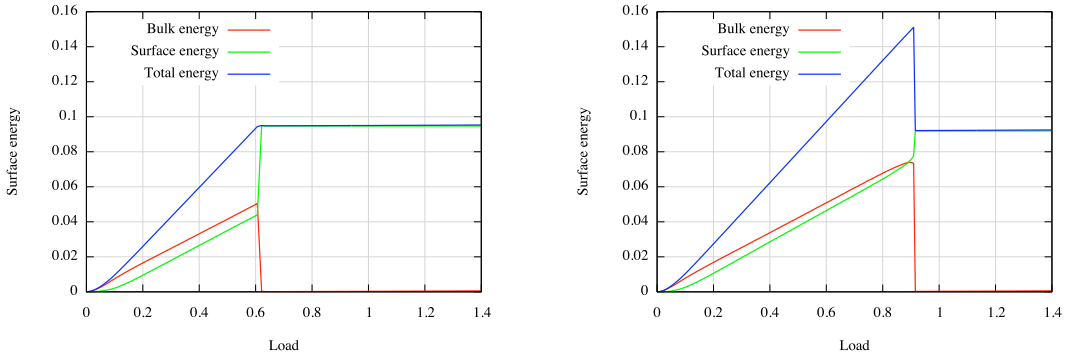

FIGURE 3. A mode-III tearing experiment: (left) global minimization leads to an unphysical evolution, (right) total energy is not conserved during "unstable" evolution.

We implemented this problem using the dynamic model presented in Section 2. In order to avoid shocks in the loading, we consider a smooth ($\mathcal{C}^1$ in time) loading given by $g(x,y;t) = g_0(t)\,\mathrm{sgn}(y)$ with

$$g_0(t) = \begin{cases} \frac{k}{2t_l}t^2 & \text{if } 0 \leq t \leq t_l, \\ kt - \frac{kt_l}{2} & \text{if } t_l \leq t \leq T, \end{cases} \tag{5}$$

t_l and T being two arbitrarily chosen thresholds with $t_l \ll T$.

In a first set of experiments, we prescribed the crack path along the symmetry axis of the domain by replacing the coupling term $\mathrm{div}\left[\left(v^2+\eta_\epsilon\right)\nabla u\right]$ in (4) with $\frac{\partial^2 u}{\partial x^2} + \frac{\partial}{\partial y}\left[\left(v^2+\eta_\epsilon\right)\frac{\partial u}{\partial y}\right]$. It is easy to see that this modification of the energy allows only discontinuities of u with normal direction (0,1) (since $\partial u/\partial x$ has to remain in L^2). We fixed the dimensions of domain ($L = 6$ and $H = 1$), the material properties ($E = 1$, $\nu = 0$, leading to $\mu = .5$, G_c=1.0E-2, and $\rho = 1$). We generated a structured mesh by decomposing the domain into squares with size h=2E-2, and subdividing each square into 4 similar triangular elements. The regularization parameters are ε=1E-2, and η_ε=1E-6. For this choice of h, ε, and G_c, the *effective toughness*, *i.e.* the surface energy associated with a discretized crack of length 1 is 1.5E-2 (see [9] for a discussion of the effective toughness). We varied the loading speed k and time T in such a way that $g_0(T) = 1.5$, and set $t_l = T/20$. We discretized the loading interval $(0,T)$ in 6,000 time steps. Figure 4 represents a typical crack evolution in this setting (the specific computation corresponds to k =5E-2). The domain is colored using the v-field, the color blue is associated to $v = 1$ (uncracked material) while the area where $v = 0$ (associated to the crack location) is colored in red.

Figure 5 represents the evolution of the surface energy as a function of time (left) and of the loading intensity $g_0(t)$ (right) for various loading velocities k ranging from 1.5E-1 to 5.0E-3. We observe that as the loading velocity decreases, the solution of the dynamic model converge to that of the quasi-static variational model, when the quasi-static model leads to progressive crack propagation. In other words, *we recover a crack evolution similar to that of the quasi-static variational formulation, when the variational formulation satisfies Griffith's criterion. Our formulation sets itself free of the paradoxes created by the quasi-static formulation while preserving its main strength, the ability to fully predict crack path, as we will see in the next experiments.* As the loading speed k increase, a larger part of the total energy gets transfered into the kinetic energy, forcing a reduction of crack length (compare the position of the crack tips *i.e.* the magnitude of the surface energy for a given load in Figure 5(right)).

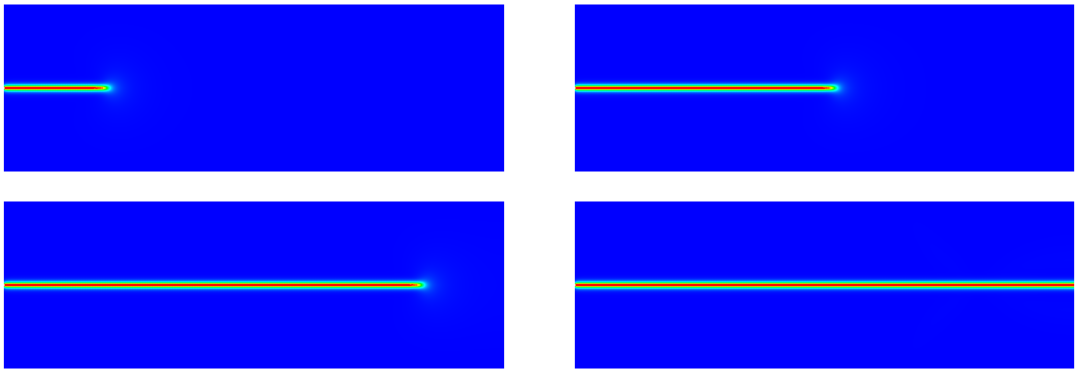

FIGURE 4. A typical crack evolution along the symmetry axis. The v–field indicates the position of the crack at $t = 6$ ($g_0 = .322$), $t = 12$ ($g_0 = .683$), $t = 18$ ($g_0 = 1.05$), and $t = 18$ ($g_0 = 1.4$).

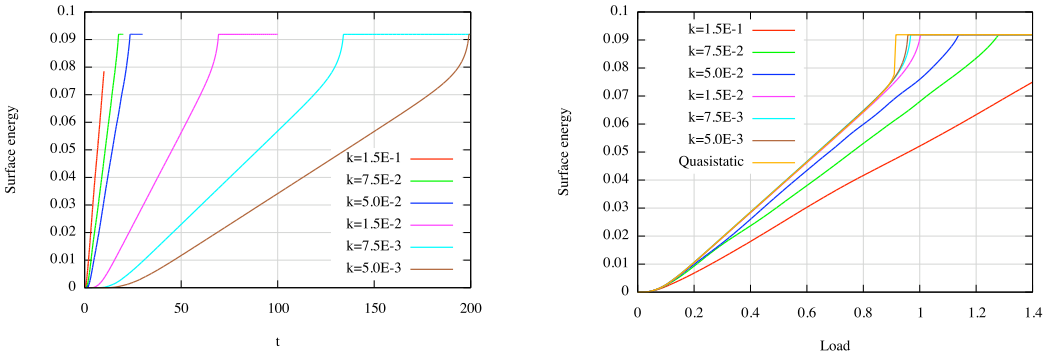

FIGURE 5. Evolution of the surface energy as a function of t (left) and of the loading g_0 (right) and for various loading speeds k.

Figure 6 represents the evolution of cracktip speed for loads in (.4,.8) as a function of the loading velocity. It is obtained by dividing the surface energy by the effective fracture toughness. For low loading velocities, the cracktip velocity depends linearly on the loading speed. This is consistent with our previous observation that our dynamic model leads to evolutions compatible with the variational approach in the low loading velocity case. Indeed from the asymptotic analysis in [9], we know that in the high aspect ratio, the surface energy is proportional to the opening magnitude. As the loading velocity increases, *the crack velocity approaches the transverse wave speed of* $1/\sqrt{2}$ *for the material we considered*. Note that the existence of a maximum crack tip velocity is hinted in Figure 5(left). As the loading speed increases, the slope of the surface energy which is proportional to the crack tip velocity seems to approach a high but finite value.

In a second set of experiments, we allow the crack to grow along arbitrary paths. Again, when the loading velocity is low enough ($k <$ 3E-2), a single crack propagates along the symmetry axis, and the crack position as a function of the loading intensity approaches that of the quasi-static case as $k \to 0$. As k increases, we observe a broader range of crack shapes. We first observe asymmetric paths where the crack starts propagating along the symmetry axis, then branches toward one of the lateral edges. Depending on the experimental conditions (including possible asymmetry of the mesh or accuracy of the linear solvers for instance), we obtain branching toward either edge. This is consistent with the fact that we do not expect the crack evolution to be unique. For faster loading velocities, we observe more complicated crack geometries involving multiple splits. Again, we stress that we did not include supplemental branching criteria to recover this expected crack behavior. As

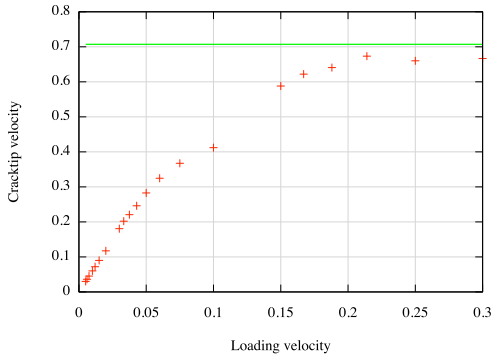

FIGURE 6. Evolution of the cracktip velocity (obtained from the surface energy) as a function of the loading speed. The green line represents the transverse wave speed for the considered material

for the variational approach to quasi-static problems, *our dynamic model leads to full crack path identification*, without additional criteria.

Figure 7 represents the crack set at $t = T$ for various loading speeds. The color coding is similar to Figure 4. Here, we use a finer mesh (h=1.0E-2) and smaller time steps (the loading phase from g_0=0 to g_0=1.5 is discretized in 12,000 time steps), while the material properties remain unchanged. The regularization parameter ε is 5.0E-3 so that the effective toughness remains unchanged from the previous set of computations. As one would exppect from a dynamic model, as the loading speed increases, one observes increasingly complicated crack patterns, including branching and splitting.

Lastly, Figure 8, represents snapshots of a crack evolution at an even higher speed (k = .15). Again, we observe multiple crack splitting and branching.

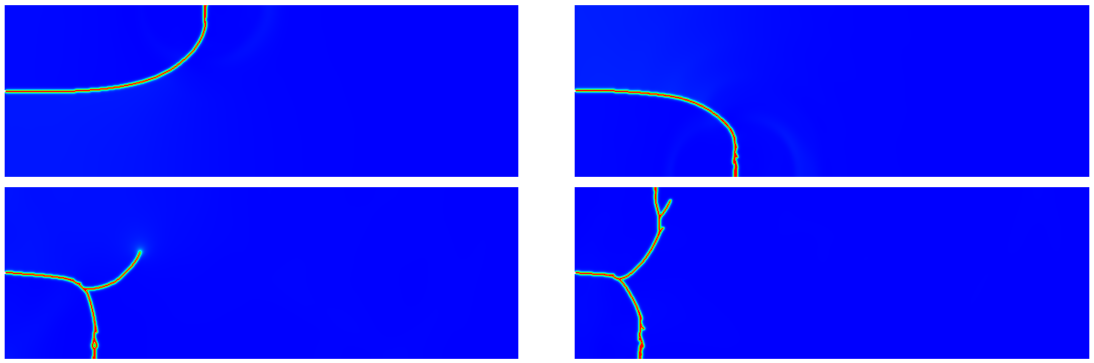

FIGURE 7. Final crack path for various loading speeds: k=3E-2 (top left), k=3.75E-2 (top right), k=4.28E-2 (bottom left), and k =5E-2 (bottom right.)

4. Conclusions and comparison with phase-field approaches

In the last few years, there have been several attempts at adapting the phase-field formalism to dynamic fracture problems. We cite in particular [4, 13, 15, 21, 22, 23, 28]. One of the main differences between our approach and the aforementioned ones come from the form of the phase-field. Ours is derived from the approximation of free-discontinuity energies devised in [2, 3], while in [4, 13, 15, 21, 22, 23], the authors introduce a phase function whose evolution is given by some variation of a gradient flow of a Ginsburg Landau–type of free energy. This type of energy is sometimes referred to in the mathematics community as the Modica-Mortola energy [29, 30]. Its

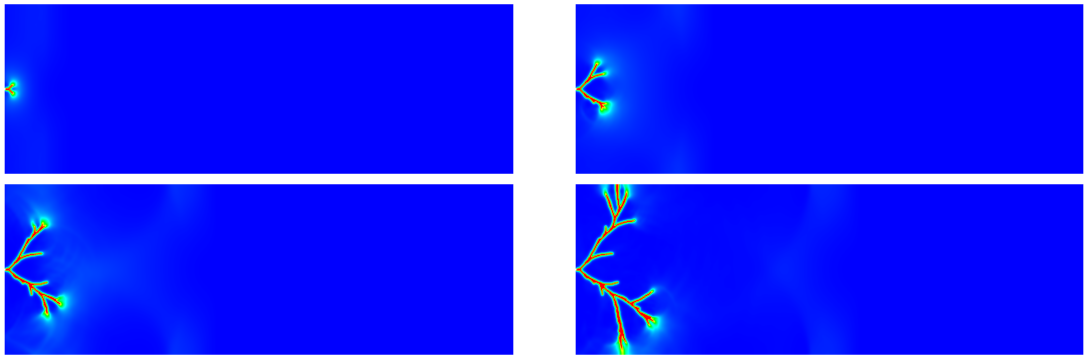

FIGURE 8. High speed loading leads to complex crack path. Snapshots of a branched crack evolution for $k = .15$ at $t = 1.20$ (g_0=2.16E-3), $t = 2.40$ (g_0=8.64E-3), $t = 3.60$ (g_0=1.94E-2), $t = 4.80$ (g_0=3.46E-2).

generic form is

$$P_\varepsilon(\phi) = \int_\Omega \left[\frac{W(\phi)}{\varepsilon} + \varepsilon |\nabla \phi| \right] dx, \tag{6}$$

where W is a double well function such that $W(0) = W(1) = 0$ and $W(x) > 0$ if $x \notin \{0, 1\}$. It is well known (see for instance [10]) that as $\varepsilon \to 0$, P_ε Γ–converges to P defined by

$$P(\phi) = \begin{cases} c\mathcal{H}^{N-1}(S(\phi)) & \text{if } u \in BV(\Omega),\ \phi \in \{0,1\} \ a.e. \\ \infty & \text{otherwise,} \end{cases} \tag{7}$$

with $c = \frac{1}{2}\int_0^1 \sqrt{W(t)}\, dt$. That is, $P(\phi) = c\mathcal{H}^{N-1}(\partial\{\phi = 0\})$, or c times the perimeter of the set where ϕ is zero. In the setting of an evolution problem, it is known that the gradient flow of (7) converges to the mean-curvature motion of almost all of its level lines, and one can estimate the normal velocity of the transition layers of ϕ (see [12]). This means that P_ε can be used to represent the length of a discontinuity set in a *free boundary* problem. However, it is not an appropriate way to model crack propagation, since crack sets are not necessarily (or even usually) the boundaries of sets. Roughly speaking, even if the field ϕ in (6) initially represents an elongated domain (say for instance $\phi(x) = 0$ if $d(x, K) \leq \eta$, where η is a given positive parameter and K is a given curve), given enough time, ϕ will evolve into a "thicker" domain.

This thickening effect is visible when looking at the evolution of a level line of the phase-field: in Figures 10 and 11 in [28], Figure 4 of [15] or Figure 3 of [22], it can be seen that the normal velocity of the level lines of the phase-field is non zero, even far away from the crack tip. Of course, the normal velocity of the crack edges is very slow compared to that of its tip, as one could expect since the gradient flow of P_ε converges to a mean curvature motion. However, as this thickening accumulates along the entire crack length, it is quite unclear if one can estimate lengths of crack increments from the variation of the free energy.

In contrast, our crack regularization formulation is derived from the regularization of a *free discontinuity* problem. In particular, it is known that if u is a discontinuous field, then as $\varepsilon \to 0$, the surface energy term F_ε Γ–converges to $\mathcal{H}^{N-1}(S(u))$. As a consequence, our approach does not suffer from the crack "thickening" effect. Indeed, as $\varepsilon \to 0$, the phase-field function v will converge to 1 almost everywhere. Formally, for any $0 \leq \alpha \leq 1$, the set $\{v \leq \alpha\}$ becomes infinitely "thin" as $\varepsilon \to 0$. Figure 9 illustrates the appropriateness of our approach to represent the evolution of a $N-1$–dimensional crack in a N–dimensional domain. Away from the crack tip, the normal velocity of the level lines of v is 0, regardless of the curvature of the crack.

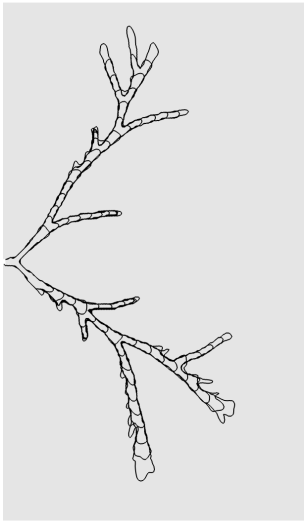

FIGURE 9. Evolution of the level line .4 of v throughout the time evolution for the computation presented in Figure 8. Note how the width of the area identified with the crack remains constant.

ACKNOWLEDGMENTS

Support for BB was provided in part by the National Science Foundation grant DMS-0605320, support for CJL was provided by National Science Foundation grants DMS-0505660 and DMS-0807825, and support for CLR was provided by the National Science Foundation grant DMS-0505660. The numerical experiments were performed using the National Science Foundation TeraGrid resources [19] provided by NCSA at the University of Illinois at Urbana-Champaign and TACC at the University of Texas under the Teragrid Resource Allocation TG-DMS060011N.

REFERENCES

[1] L. Ambrosio and A. Braides. Energies in SBV and variational models in fracture mechanics. In *Homogenization and applications to material sciences (Nice, 1995)*, volume 9 of *GAKUTO Internat. Ser. Math. Sci. Appl.*, pages 1–22. Gakkōtosho, Tokyo, 1995.

[2] L. Ambrosio and V.M. Tortorelli. Approximation of functionals depending on jumps by elliptic functionals via Γ-convergence. *Comm. Pure Appl. Math.*, 43(8):999–1036, 1990.

[3] L. Ambrosio and V.M. Tortorelli. On the approximation of free discontinuity problems. *Boll. Un. Mat. Ital. B (7)*, 6(1):105–123, 1992.

[4] I.S. Aranson, V.A. Kalatsky, and V.M. Vinokur. Continuum field description of crack propagation. *Phys. Rev. Lett.*, 85(1):118–121, Jul 2000.

[5] S. Balay, K. Buschelman, V. Eijkhout, W. D. Gropp, D. Kaushik, M. G. Knepley, L. C. McInnes, B. F. Smith, and H. Zhang. PETSc users manual. Technical Report ANL-95/11 - Revision 2.1.5, Argonne National Laboratory, 2004.

[6] S. Balay, K. Buschelman, W.D. Gropp, D. Kaushik, M. G. Knepley, L. C. McInnes, B. F. Smith, and H. Zhang. PETSc Web page, 2001. http://www.mcs.anl.gov/petsc.

[7] B. Bourdin. Numerical implementation of the variational formulation for quasi-static brittle fracture. *Interfaces Free Bound.*, 9(3):411–430, 2007.

[8] B. Bourdin, G. A. Francfort, and J.-J. Marigo. Numerical experiments in revisited brittle fracture. *J. Mech. Phys. Solids*, 48(4):797–826, 2000.

[9] B. Bourdin, G.A. Francfort, and J.-J. Marigo. *The Variational Approach to Fracture*. Springer, 2008.

[10] A. Braides. *Approximation of Free-Discontinuity Problems*. Number 1694 in Lecture Notes in Mathematics. Springer, 1998.

[11] A. Braides. Γ-*convergence for beginners*, volume 22 of *Oxford Lecture Series in Mathematics and its Applications*. Oxford University Press, Oxford, 2002.

[12] L. Bronsard and R.V. Kohn. On the slowness of phase boundary motion in one space dimension. *Comm. Pure Appl. Math.*, 43(8):983–997, 1990.

[13] F. Corson, M. Adda-Bedia, H. Henry, and E. Katzav. Thermal fracture as a framework for crack propagation law. Preprint arXiv:0801.2101v1, 2008.

[14] G. Dal Maso. *An introduction to* Γ-*convergence*. Birkhäuser, Boston, 1993.

[15] L.O. Eastgate, J.P. Sethna, M. Rauscher, T. Cretegny, C.-S. Chen, and C.R. Myers. Fracture in mode i using a conserved phase-field model. *Phys. Rev. E*, 65(3):036117, Feb 2002.
[16] G. A. Francfort and C. J. Larsen. Existence and convergence for quasi-static evolution in brittle fracture. *Comm. Pure Appl. Math.*, 56(10):1465–1500, 2003.
[17] G. A. Francfort and J.-J. Marigo. Revisiting brittle fracture as an energy minimization problem. *J. Mech. Phys. Solids*, 46(8):1319–1342, 1998.
[18] A. Giacomini. Ambrosio-Tortorelli approximation of quasi-static evolution of brittle fractures. *Calc. Var. Partial Differential Equations*, 22(2):129–172, 2005.
[19] L. Grandinetti, editor. *TeraGrid: Analysis of Organization, System Architecture, and Middleware Enabling New Types of Applications*. Advances in Parallel Computing. IOS Press, Amsterdam, 2007.
[20] A.A. Griffith. The phenomena of rupture and flow in solids. *Philosophical Transactions of the Royal Society of London*, 221:163–198, 1921.
[21] V. Hakim and A. Karma. Laws of crack motion and phase-field models of fracture. *J. Mech. Phys. Solids*, In Press, Corrected Proof:–, 2008.
[22] A. Karma, D.A. Kessler, and H. Levine. Phase-field model of mode III dynamic fracture. *Phys. Rev. Lett.*, 87(4):045501, Jul 2001.
[23] A. Karma and A.E. Lobkovsky. Unsteady crack motion and branching in a phase-field model of brittle fracture. *Physical Review Letters*, 92(24):245510, 2004.
[24] D.E Keyes, D.R. Reynolds, and C.S. Woodward. Implicit solvers for large-scale nonlinear problems. *Journal of Physics: Conference Series*, 46:433–442, 2006.
[25] C. J. Larsen, C. Ortner, and E. Süli. A phase field approach to dynamic fracture: existence and convergence. in progress.
[26] C.J. Larsen. Models for Dynamic Fracture Based on Griffith's Criterion. In *IUTAM Symposium on Variational Concepts with Applications to the Mechanics of Materials*, to appear.
[27] B. Lawn. *Fracture of Brittle Solids (2nd ed)*. Cambridge University Press, 1993.
[28] V. I. Marconi and E. A. Jagla. Diffuse interface approach to brittle fracture. *Phys. Rev. E*, 71(3):036110, 2005.
[29] L. Modica and S. Mortola. Il limite nella Γ–convergenza di una famiglia di funzionali ellittici. *Boll. Un. Mat. Ital. A (5)*, 14(3):526–529, 1977.
[30] L. Modica and S. Mortola. Un esempio di Γ–convergenza. *Boll. Un. Mat. Ital. B (5)*, 14(1):285–299, 1977.

(Blaise Bourdin) Department of Mathematics, Louisiana State University, Baton Rouge, LA 70803, USA
E-mail address: bourdin@lsu.edu

(Christopher J. Larsen) Department of Mathematical Sciences, Worcester Polytechnic Institute, 100 Institute Road, Worcester MA 01609-2280, USA
E-mail address: cjlarsen@wpi.edu

(Casey L. Richardson) UCLA Mathematics Department Box 951555 Los Angeles, CA 90095-1555, USA
E-mail address: clr@math.ucla.edu